Anomalous Radiative Transfer in Heterogeneous Media

ADVANCED THEORY AND SIMULATIONS
www.advtheorysimul.com

Anomalous Radiative Transfer in Heterogeneous Media

Federico Tommasi, Lorenzo Pattelli, Stefano Cavalieri, Lorenzo Fini, Michela Paolucci, Ernesto Pini, Angelo Sassaroli, and Fabrizio Martelli**

Monte Carlo (MC) simulations are the gold standard for describing various transport phenomena and have largely contributed to the understanding of these processes. However, while their implementation for classical transport governed by exponential step-length distributions is well-established, widely accepted approaches are still lacking for the more general class of anomalous transport phenomena. In this work, a set of rules for performing MC simulations in anomalous diffusion media is identified, which is also applicable in the case of finite-size geometries and/or heterogeneous inclusions. The results are presented in the context of radiative transfer, however their implications extend to all types of anomalous transport. The proposed set of rules exhibits full compatibility with the pathlength invariance property for random trajectories, and with the important radiometric concept of fluence. Additionally, it reveals the counter-intuitive possibility of introducing interfaces between independent subdomains with identical properties, which arise from the fact that non-exponential step-length distributions have a "memory" that can in principle be reset when traversing a boundary. These results have far-reaching consequences not just for the physical interpretation of the corrections required to handle these discontinuities, but also for their experimental verification, due to their expected effects on the observable pathlength distributions.

1. Introduction

The relevance of the Monte Carlo (MC) method for the study of transport phenomena can hardly be overstated. This simple algorithm is used seamlessly to describe the propagation of heat,[1] particles,[2] living organisms,[3] as well as light from the scale of small biological tissues[4] to atmospheric physics[5] and entire galaxies.[6]

In many cases, transport is modeled assuming a chain of independent scattering events, leading to an exponential distribution of waiting times or step lengths.[7] However, in reality, several transport phenomena take place in complex environments that introduce statistical correlations between scattering centers,[8] and hence a dependence on the previous history of the random walk that cannot be described by the memoryless exponential distribution.[9] Indeed, non-exponential step lengths are deeply rooted in the study of these processes: the very theory of random walks was first developed for normally-distributed step lengths to model stock market fluctuations,[10] and the term itself "random walk" was coined to describe the diffusion of mosquitoes assuming fixed-length steps.[11] To date, countless more examples are known of non-exponential step length distributions, including notable examples such as Mittag-Leffler step functions[12] or Lévy walks,[13] which have been identified in the mobility patterns of bacteria,[14] humans,[15] eye movements,[16] as well as in the propagation of cosmic rays[17] and light,[18] to name a few.

Extending the Monte Carlo method to the non-exponential case seems as trivial as replacing the step length distribution with the desired function. While this is indeed sufficient for the description of trajectories in an unbounded medium, handling reflections or crossings at boundaries is less trivial for functions that are not memoryless. Sample boundaries can in fact occur at uncorrelated positions compared to scattering events, breaking the chain of correlated step lengths, and hence resetting their memory.

Reciprocity considerations indicate that the length distribution of any step stemming from a boundary should be the same as that of the steps which terminate at a boundary.[19–23] Following this principle, the fundamental invariance property (IP) of random trajectories is also automatically fulfilled for all types of step length distributions.[20,24–28] Nonetheless, the important difference between scattering and boundary events is typically ignored in the vast majority of Monte Carlo studies of anomalous

F. Tommasi, S. Cavalieri, L. Fini, M. Paolucci, E. Pini, F. Martelli
Dipartimento di Fisica e Astronomia
Università degli Studi di Firenze
via Giovanni Sansone 1, Sesto Fiorentino 50019, Italy
E-mail: fabrizio.martelli@unifi.it

L. Pattelli
Istituto Nazionale di Ricerca Metrologica (INRiM)
Str. delle Cacce 91, Turin 10135, Italy
E-mail: l.pattelli@inrim.it

L. Pattelli, E. Pini
European Laboratory for Non-linear Spectroscopy (LENS)
via Nello Carrara 1, Sesto Fiorentino 50019, Italy

A. Sassaroli
Department of Biomedical Engineering
Tufts University
4 Colby Street, Medford, Massachusetts 02155, USA

The ORCID identification number(s) for the author(s) of this article can be found under https://doi.org/10.1002/adts.202400182

[Correction added on 23 December, 2024 after online publication: The copyright line for this article was changed in this version.]

DOI: 10.1002/adts.202400182

transport, where only one step length distribution is used to generate trajectories inside a given material.[12,29–33]

In this work, starting from the generalized radiative transfer equation (GRTE),[34–36] we formulate and verify an extension of the Monte Carlo method to anomalous light transport in media with arbitrary inhomogeneities, which has important consequences for the representation of scattering volumes through mesh or voxel discretizations, as well as for the interpretation of experimental data. Our results show that modified statistical distributions must be employed not just for the initial step entering a scattering domain,[21,23] but also each time a trajectory interacts with a boundary, an effect that can be largely magnified by the presence of refractive index discontinuities between different subdomains. The validity of our approach is supported by its full consistency with the invariance property and, for the first time in the case of non-exponential propagation, by a direct comparison with the fluence rate inside each scattering subdomain, which represents the fundamental radiometric quantity for the description of light transport.[37]

2. Monte Carlo Simulations

To date, an organic theory of anomalous transport has only been developed for the infinite medium,[34–36] which raises the critical issue of handling boundaries in anomalous transport. In this work, previous studies on the generalized radiative transfer equation are extended by identifying a set of rules for performing Monte Carlo simulations in heterogeneous anomalous media with boundaries. The resulting set of rules has broad generality, encompassing also the classical transport as a special case.

In a scattering medium, a boundary is any interface demarcating regions with different properties. This includes both the outer interface between the medium and its host environment, as well as any internal interface between different regions. The correct energy balance must be enforced at any boundary, connecting the specific intensity in the two adjacent regions according to radiative transfer. In the MC picture, this requires to define how trajectories, which carry energy, interact with such boundaries. Since the GRTE is a generalization of the classical radiative transfer equation (RTE), an implementation of generalized MC simulations can be built based on the classical MC approach,[23] with two main modifications:

- non-exponential step length distributions can be used to generate steps taken inside the scattering medium, instead of the exponential distribution predicted by the Beer-Lambert-Bouguer law of the classical RTE;
- since in the GRTE the location of scattering centers can be correlated, any interaction with a boundary separating different regions will also reset the memory of a trajectory, requiring the generation of an uncorrelated step length.[20,21,23]

The second rule follows from the assumption that the position of a medium boundary should be independent of the position of the scattering centers inside it. This implies that boundary interactions can occur at uncorrelated positions with any previous scattering event, thus resetting the memory of the non-exponential step length distribution. Although some of these general considerations have been already outlined in the previous literature, they are extended here to the case of heterogeneous media with internal sub-domains, offering a direct illustration of their expected consequences for experimentally observable quantities. The identified set of rules is universal, as it can be seamlessly applied to the special case of classical RTE, by assuming an exponential step length distribution.

Without loss of generality, a spherical geometry with different domains arranged as concentric shells is considered. The term $p_c(\ell)$ refers to the "correlated" step length distribution associated to the bulk of a scattering domain (characterized by homogeneous properties), while the term $p_u(\ell)$ is used to identify "uncorrelated" steps originating from a boundary of that domain. **Figure 1** depicts an example of a trajectory in a scattering medium encompassing multiple domains, highlighting the different distributions required to generate steps that originate within the medium or at one of its interfaces.

Given a certain distribution p_c, its corresponding p_u can be calculated as:[21,23,38]

$$p_u(\ell) = \frac{1 - \int_0^\ell p_c(\ell')\,d\ell'}{\int_0^\infty \ell' p_c(\ell')\,d\ell'} = \frac{1 - \int_0^\ell p_c(\ell')\,d\ell'}{\langle \ell \rangle} \tag{1}$$

which is connected to the "survival function" of a probability distribution, and ensures that steps departing from a boundary have the same probability distribution of steps that are terminated by a boundary interaction. As a consequence, it can be shown that the application of this rule satisfies both the invariance property and reciprocity.[19–23] Equation (1) implies this, even though it is formally defined only for distributions having a finite first moment. Therefore, simulating trajectories in anomalous media requires the use of two different distributions: one for scattering events within the medium, and one for steps stemming from a boundary.

Several examples of non-exponential distributions have been used in the literature to describe anomalous transport of light, such as Mittag-Leffler or Lévy stable distributions.[12,13,17,18,39,40] In this work, without loss of generality, the generalized Pareto distribution (GPD) is adopted, which is sometimes applied in economy[41] and ecology.[42] This choice is motivated by several factors. First, the GPD conveniently admits closed-form expressions for all distributions of interest, including p_c^{GP}, p_u^{GP}, but also their inverse cumulative distribution functions that are needed for efficient random variate generation. Second, the GPD can be parameterized by a scale parameter σ and a shape parameter k to generate a whole family of distributions:

$$p_c^{GP}(\ell) = \frac{1}{\sigma} \begin{cases} \left(1 + \frac{k\ell}{\sigma}\right)^{-(k+1)/k} & k > 0 \\ e^{-\ell/\sigma} & k = 0 \end{cases} \tag{2}$$

comprising also the classical (exponential) case for $k = 0$. For $k > 0$, the distribution becomes fat-tailed, with a diverging variance for $k \geq 0.5$, and even a diverging first moment for $k \geq 1$. This can be seen from the relation linking the parameters k and σ to the mean value $\langle \ell \rangle$, that is the reciprocal of the scattering coefficient μ_s

$$\langle \ell \rangle = \mu_s^{-1} = \frac{\sigma}{1-k} \qquad \text{for } k < 1 \tag{3}$$

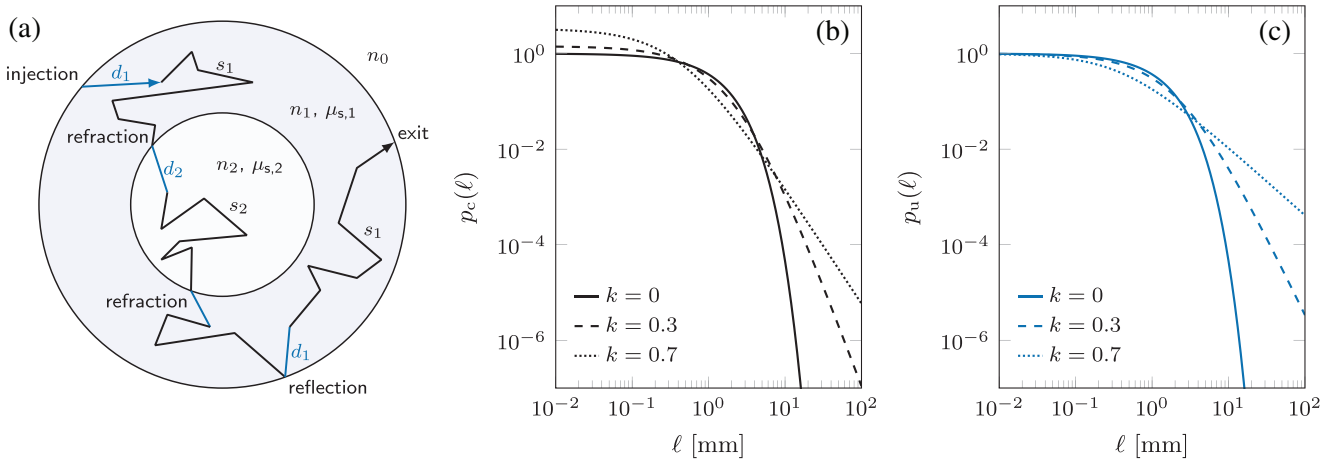

Figure 1. a) Propagation of a trajectory in an illustrative anomalous medium comprising two regions with different scattering coefficients μ_{s1} and μ_{s2} and refractive indices n_1 and n_2. The external environment has a refractive index n_0. Step lengths $s_{1,2}$ inside the scattering domain are extracted according to $p_c(\ell)$ distributions (black). Steps departing from a boundary (either at the injection point, or following refraction or reflection events) are extracted with $p_u(\ell)$ distributions (blue). b) Comparison between exponential ($k = 0$) and non-exponential ($k \neq 0$) p_c distributions taken from the family of generalized Pareto distributions with equal mean step value $\langle \ell \rangle = 1$ mm. c) Comparison between the corresponding $p_u(\ell)$ derived as the survival functions of the respective $p_c(\ell)$. For the exponential case we have that $p_c(\ell) = p_u(\ell)$.

Hence, for $k < 1$, it is possible to perform simulations with different shape parameters k while keeping the same scattering coefficient μ_s. In this context, this parameter borrows its meaning from the classical derivation in radiative transfer,[43] and provides an indication of the rate of scattering events inside the medium. Finally, by substituting Equation (2) into Equation (1) and calculating the survival function, $p_u^{GP}(\ell)$ is written as:

$$p_u^{GP}(\ell) = \mu_s(1 + k\ell/\sigma)^{-\frac{1}{k}} \qquad k > 0 \tag{4}$$

A useful property of the GPD, is that it admits simple analytical expressions for the cumulative distributions of both its probability density functions p_c^{GP} and p_u^{GP}. For $1 > k > 0$, these can be written as:

$$P_c^{GP}(\ell) = 1 - (1 + k\ell/\sigma)^{-\frac{1}{k}} \tag{5}$$

$$P_u^{GP}(\ell) = 1 - (1 + k\ell/\sigma)^{1-\frac{1}{k}} \tag{6}$$

Even more conveniently for MC simulations, both Equation (5) and (6) can be inverted to give their respective quantile functions, from which random correlated and uncorrelated step lengths can be generated passing a uniformly distributed random argument $\xi \in (0, 1)$:

$$\ell_c^{GP}(\xi) = \frac{1-k}{k\mu_s}(\xi^{-k} - 1) \tag{7}$$

$$\ell_u^{GP}(\xi) = \frac{1-k}{k\mu_s}\left(\xi^{k/(k-1)} - 1\right) \tag{8}$$

while for $k = 0$ the Beer-Lambert-Bouguer case is recovered, which is characterized by $p^{BLB}(\ell) = \mu_s \exp(-\mu_s\ell)$ and $P^{BLB}(\ell) = 1 - \exp(-\mu_s\ell)$, hence:[43]

$$\ell_c^{BLB}(\xi) = \ell_u^{BLB}(\xi) = -\frac{\ln \xi}{\mu_s} \tag{9}$$

The two distributions p_c^{GP} and p_u^{GP} are the main building blocks for the implementation of MC simulations in anomalous media. For a generalized Pareto step length distribution, in fact, Equation (7) can be used to draw random lengths for steps taken inside a scattering domain, while Equation (8) should be used whenever the step stems from a boundary. In the first case, the step will retain a memory of the distance from the previous scattering event. In the second case, this memory is effectively reset by the boundary interaction. The use of a discontinuous distribution based on the survival function (1) was originally proposed to describe only the initial step length inside an anomalous scattering domain in an otherwise homogeneous medium.[20–22] In the presence of any internal heterogeneity (including, e.g., refractive index, scattering coefficient, or scattering function discontinuities among different sub-domains), the same rule must be applied to any step departing from a boundary, leading to a more significant modification of the distribution of step lengths forming each trajectory.

The correctness of this approach is verified in different configurations by checking its consistency against two important invariant properties that are expected to hold for general random walks. In the context of light transport, the first Invariance Principle (IP), or Cauchy formula,[19,20,24,25,28,44–48] states that the total average path length $\langle L \rangle$ for light traveling through a non-absorbing medium of refractive index n under homogeneous and isotropic illumination conditions (Lambertian illumination) depends only on the ratio between its volume V and surface S, and its refractive index contrast, n/n_0, with the environment (n_0), as:[27,48]

$$\langle L \rangle = 4\frac{V}{S}\frac{n^2}{n_0^2} = \langle L \rangle_{IP} \tag{10}$$

Equation (10) can be generalized to the case of heterogeneous media made of discrete sub-volumes V_i with refractive indices n_i as:[27]

$$\langle L \rangle = \frac{4}{Sn_0^2}\sum_i V_i n_i^2 = \sum_i \langle L_i \rangle_{IP} \tag{11}$$

The second invariant is built upon the fluence rate $\Phi(\boldsymbol{r}) = \int_{4\pi} I(\boldsymbol{r}, \mathbf{s})\, \mathrm{d}\mathbf{s}$, defined as the specific intensity in $\boldsymbol{r}$, $I(\boldsymbol{r}, \mathbf{s})$, integrated along all directions $\mathbf{s}$. Under Lambertian illumination, invariant solutions of the RTE in each sub-domain exist,[27] which can be expressed as:

$$\Phi_i(\boldsymbol{r}) = 4\pi I_{\mathrm{in}} \frac{n_i^2}{n_0^2} \qquad \forall \boldsymbol{r} \in V_i \tag{12}$$

where I_{in} is the constant isotropic radiance impinging on the medium.

For classical transport, it is well known that the average fluence $\langle \Phi_i \rangle$ in a sub-volume V_i can be connected to the average total path length $\langle L_i \rangle$ spent by all trajectories inside the same sub-volume:[37]

$$\langle \Phi_i \rangle = \frac{P_{\mathrm{e}}}{V_i} \langle L_i \rangle \tag{13}$$

where P_{e} is the total power emitted by all light sources illuminating the medium. In contrast with the average pathlength, the photon fluence rate is a fundamental and experimentally measurable radiometric quantity in radiative transfer that is largely employed to describe light transport in several applications.[49–51] This conceptually independent verification is intimately connected with the foundations of radiative transfer theory, and has never been reported for the case of anomalous transport.

The consistency of two alternative MC implementations is verified against both invariant quantities. In the first implementation, all random step lengths are generated with the same target distribution, using Equation (7). This corresponds to the mainstream approach used in classical media,[27,47] which has been also extended to describe MC simulations of anomalous transport.[12,29–32] In the second implementation, Equation (7) is used to handle interactions occurring in the bulk of a scattering domain, while Equation (8) is used to generate random steps following a boundary interaction. The numerical verification provides insights on the correct modeling of boundaries in anomalous radiative transport (ART), for which a theoretical description is not yet available.

3. Results

Monte Carlo simulations are performed on spherically symmetric samples with a variable number of concentric shells and fixed external radius of 5 mm. Spherical symmetry is particularly convenient for the practical realization of a Lambertian and isotropic illumination associated to the validity of the IP, as it allows to initialize all trajectories at a single injection point, with an entrance angle randomly drawn from a cosine distribution.[27,43] Similarly, under this spherical symmetry condition, the fluence rate can be calculated as a function of $|\boldsymbol{r}|$ in each concentric shell.

Simulation results are shown for a broad range of scattering coefficient, i.e., $\mu_{\mathrm{s}} \in [10^{-4}, 10^{1}]$ mm^{-1}, and for isotropic scattering ($g = 0$). Equivalent results were obtained by setting a phase function with a finite anisotropy factor, consistently with the independence of the IP on the scattering properties.

Shape parameter values of $k = 0.3$ and 0.7 have been selected for the GP step length distribution, to study two different anomalous transport cases with finite and diverging variance. For each configuration, 10^2 simulations with 10^5 trajectories have been run and averaged to estimate mean values with their standard errors.[47]

3.1. Mean Path Length and Fluence

The mean value of the total path length spent inside the medium by the escaped trajectories, $\langle L \rangle$, and its corresponding standard error are shown in **Figure 2** for homogeneous and layered geometries with different types of discontinuities. Calculated values are normalized by the IP prediction given by Equation (11).

A first configuration (Figure 2a,d) shows the case of a homogeneous sphere with refractive index $n_1 = 1.4$ in an environment with $n_0 = 1$. The value predicted by the IP is $\langle L \rangle_{\mathrm{IP}} = 13.0\bar{6}$ mm, in excellent agreement with the value obtained using the discontinuity step at boundaries, for all values of μ_{s}. In the ballistic regime ($\mu_{\mathrm{s}} \to 0$ mm^{-1}), both methods converge to the correct value, irrespective of how boundaries are handled. This is expected since, in the absence of scattering, all trajectories converge to the ballistic regime, which fulfils trivially the IP via the mean chord length theorem.[43,44,52] Above a certain scattering strength, however, significant deviations arise when using only ℓ_{c}, exceeding 40% for $k = 0.7$ and $\mu_{\mathrm{s}} = 10$ mm^{-1}. This large discrepancy emerges despite the homogeneous geometry, largely due to the presence of a refractive index contrast at the external boundary, which causes some trajectories to be reflected multiple times inside the scattering medium, thus significantly increasing the number of uncorrelated step lengths.

Similar results are obtained also for the layered configurations. Two cases are considered comprising equal-volume concentric shells with alternating refractive indices (Figure 2b,e), or with an alternation of both n_i and $\mu_{\mathrm{s},i}$ (Figure 2c,f), showing good agreement of the proposed strategy for all degrees of scattering.

In **Figure 3**, the results of anomalous MC simulations are compared against the benchmark fluence prediction given by Equation (12) for a 10-layered sphere with graded refractive index.

Given their constant refractive index n_i, Equation (12) predicts a constant invariant fluence rate Φ_i in every point of each layer, which can be used to verify the correctness of an MC estimation based on the intrinsic definition of the fluence rate.[43] Exploiting the spherical symmetry of the system under study, this quantity can be conveniently calculated at any position $\boldsymbol{r}$ inside the scattering medium by performing a normalized summation of the contributions to the fluence from all simulated trajectories passing through a spherical surface of radius $|\boldsymbol{r}|$.[43,49] In Figure 3b,d, the resulting values are further checked for consistency against the average fluence rates $\langle \Phi_i \rangle$ calculated using Equation (13). The results of MC simulations using the uncorrelated step after each boundary interaction are in excellent agreement with the expected values, which further confirms the validity of a direct relation between fluence and mean pathlength also in the context of ART. Identical conclusions can be reached when considering the full radiance distributions at each spherical interface and its invariance characteristics.[27] For the sake of brevity, this additional analysis is not shown, however all radiance distributions are included in the supporting data repository.

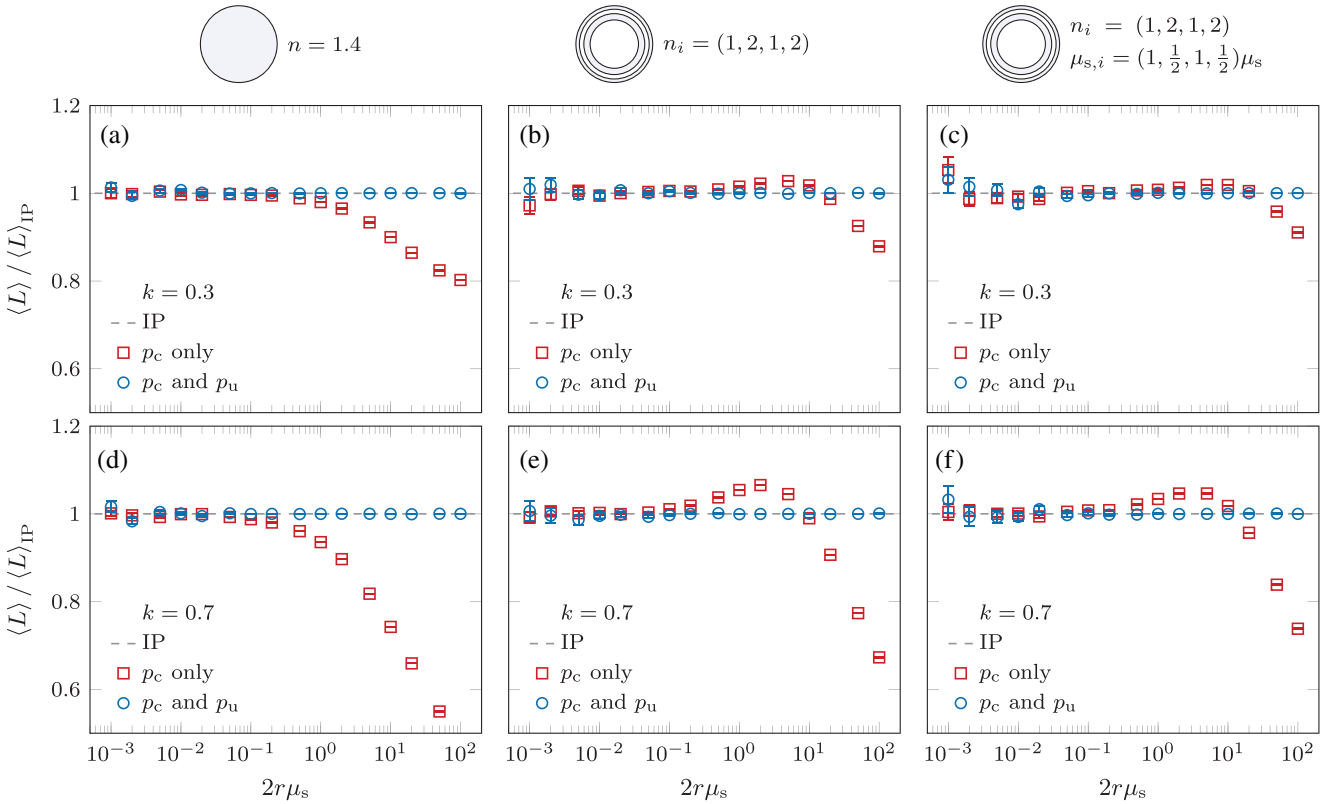

Figure 2. Total $\langle L \rangle$ spent inside a non-absorbing sphere of radius $r = 5$ mm, surrounded by a non-scattering region of unit refractive index, illuminated by a Lambertian source, normalized to the IP prediction, $\langle L \rangle_{IP}$. For each value of μ_s, three configurations are studied: a homogeneous case with a refractive index contrast with the external environment (panels a, d); a 4-layered sphere with alternating refractive indices n_i (b, e); and a 4-layered sphere with alternating indices n_i and scattering coefficients $\mu_{s,i}$ (c, f). The index i indicates the layers from the inside to the outside of the sphere. The gray dashed line indicates the IP prediction. Blue and red symbols refer to MC simulations obtained with and without the use of Equation (1) after interface events.

3.2. Total Pathlength Distributions

To gain a deeper insight on the effect of discontinuities on anomalous light transfer, it is instructive to study their impact on the probability density function of total pathlengths, $p(L)$. The complete distributions, in fact, can reveal significant differences that are not apparent when considering only their expectation value $\langle L \rangle$ (i.e., the IP).

Figure 4 summarizes the results obtained for two configurations without (Figure 4a,c) and with (Figure 4b,d) refractive index contrast at the external boundary.

In the index-matched case (which is notably the sole configuration that has been discussed up to now in the literature), only the initial step (i.e., photon injection) of each trajectory is affected by the uncorrelated distribution (8). As a consequence, it can be expected that all macroscopic transport properties for the propagation of light inside this configuration remain unaffected between the two MC approaches. Indeed, only a small correction is observed between pairs of distributions (as required to fulfill the IP condition), while the decay rate of both distributions is otherwise equal.

On the other hand, a very different scenario is observed when a refractive index mismatch is introduced at the sphere boundary. In this case, fulfilling the IP condition (cfr. Figure 4b,d) involves a modification of the whole pathlength distribution. This modification involves not just the appearance of a prominent peak at $p(L = 0 \text{ mm})$ due to the intensity that is specularly reflected at the external interface (which must be taken into account for the correct verification of the IP), but also an appreciable change to the decay rates in the multiple scattering regime. While the magnitude of the peak at $L = 0$ mm depends only on the refractive index mismatch, and hence is unaffected by the choice of the step length distribution taken at boundaries, the amount of internal reflections of light entering the medium is strongly enhanced with increasing turbidity, resulting in a larger influence of the uncorrelated step lengths over the total pathlength distribution which eventually balances the $p(L = 0 \text{ mm})$ peak exactly.

This observation is particularly relevant for the possible experimental verification of the proposed set of rules, as it suggests that major differences should be expected in the tails of the pathlength distribution of index-mismatched anomalous media, which are directly measurable using several experimental techniques.[53–56]

3.3. Generalized Boundaries in Anomalous Transport

Based on the above considerations, it is instructive to consider one last type of configuration leading to an apparently counter-intuitive behavior. As we have discussed, traversing an interface

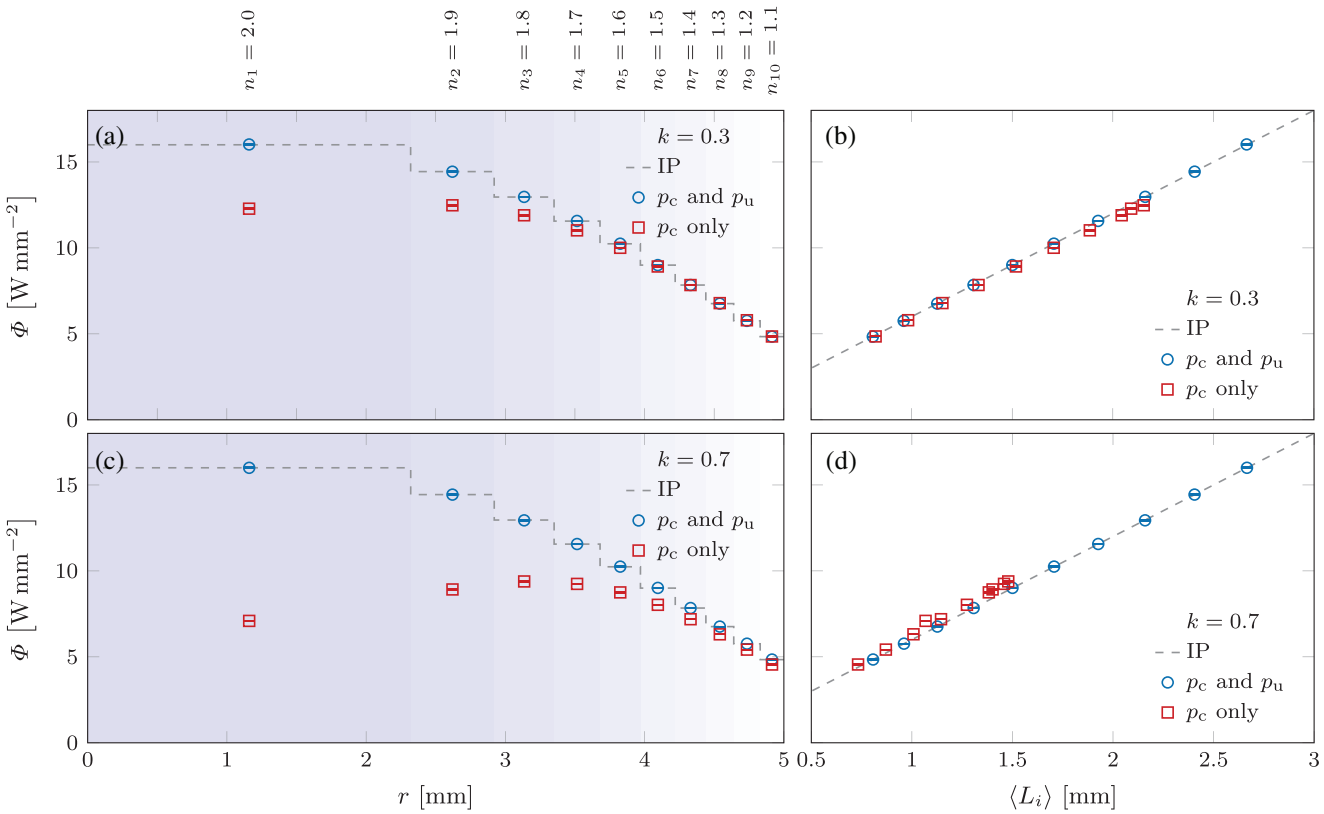

Figure 3. a,c) Fluence rate Φ in each sub-volume of a ten-layered sphere of radius 5 mm with refractive index discontinuities (values shown on top) and constant scattering $\mu_s = 2$ mm^{-1}. The gray dashed line represents the values predicted by Equation (12). b,d) Comparison between the fluence rate Φ and the average total pathlength $\langle L_i \rangle$ of all trajectories inside each layer.

between two materials (having either different step length distribution, refractive index, scattering coefficient, or scattering function) is a sufficient condition to require that step lengths are reset after interacting with the boundary. However, in principle, the same rule should be applied also at the interface between two independent realizations of the same anomalous material sharing the same optical properties on both sides of the boundary. Hence, it is worth comparing the case of a homogeneous domain with that of the same domain arbitrarily split into multiple subdomains with equal properties. This is not an abstract exercise, as it corresponds, for instance, to a case where two or more independent realizations of the same anomalous material (e.g., a Lévy glass) are optically glued together to form a single multidomain sample.

This configuration is interesting as we know that the proposed set of rules satisfies all invariant solutions in the homogeneous configuration, and that introducing boundaries does produce an impact on the total pathlength distributions. This raises the question whether introducing this type of arbitrary or generalized boundaries inside an otherwise homogeneous domain can lead to pathlength modifications that are still compatible with the desired invariants.

Figure 5a shows the pathlength distributions $p(L)$ obtained for five different configurations of a sphere with identical size and optical properties ($r = 5$ mm, $k = 0.7$, $n/n_0 = 1.4$, $\mu_s = 1$ mm^{-1}), divided into a variable number of equivalent domains.

As expected, the introduction of arbitrary interfaces inside the anomalous medium has a direct and measurable impact on the probability of observing trajectories of different lengths, as dictated by the altered balance of each trajectory in terms of their composition of continuous and discontinuous steps.

Interestingly, however, this change is such that the validity of the IP remains unaltered (Figure 5b). This result shows that, albeit necessary, a mere verification of the IP is not a particularly stringent condition for all aspects of propagation, as it can be fulfilled by an infinite set of different pathlength distributions. Conversely, considering the whole $p(L)$ distributions provides important insights into the dynamics of anomalous transport that would otherwise remain concealed, and suggest promising strategies for experimental validation and physical interpretation of the set of rules needed to handle boundary interactions in MC simulations.

4. Conclusion

In this work, we verified a set of rules for the description of boundary interactions in Monte Carlo simulations of heterogeneous media with non-exponential step length distributions, which are relevant for the accurate description of anomalous transport processes. The investigated set of rules extends previous works by *i*) including the general case of refractive index discontinuities among different subdomains or with the embedding

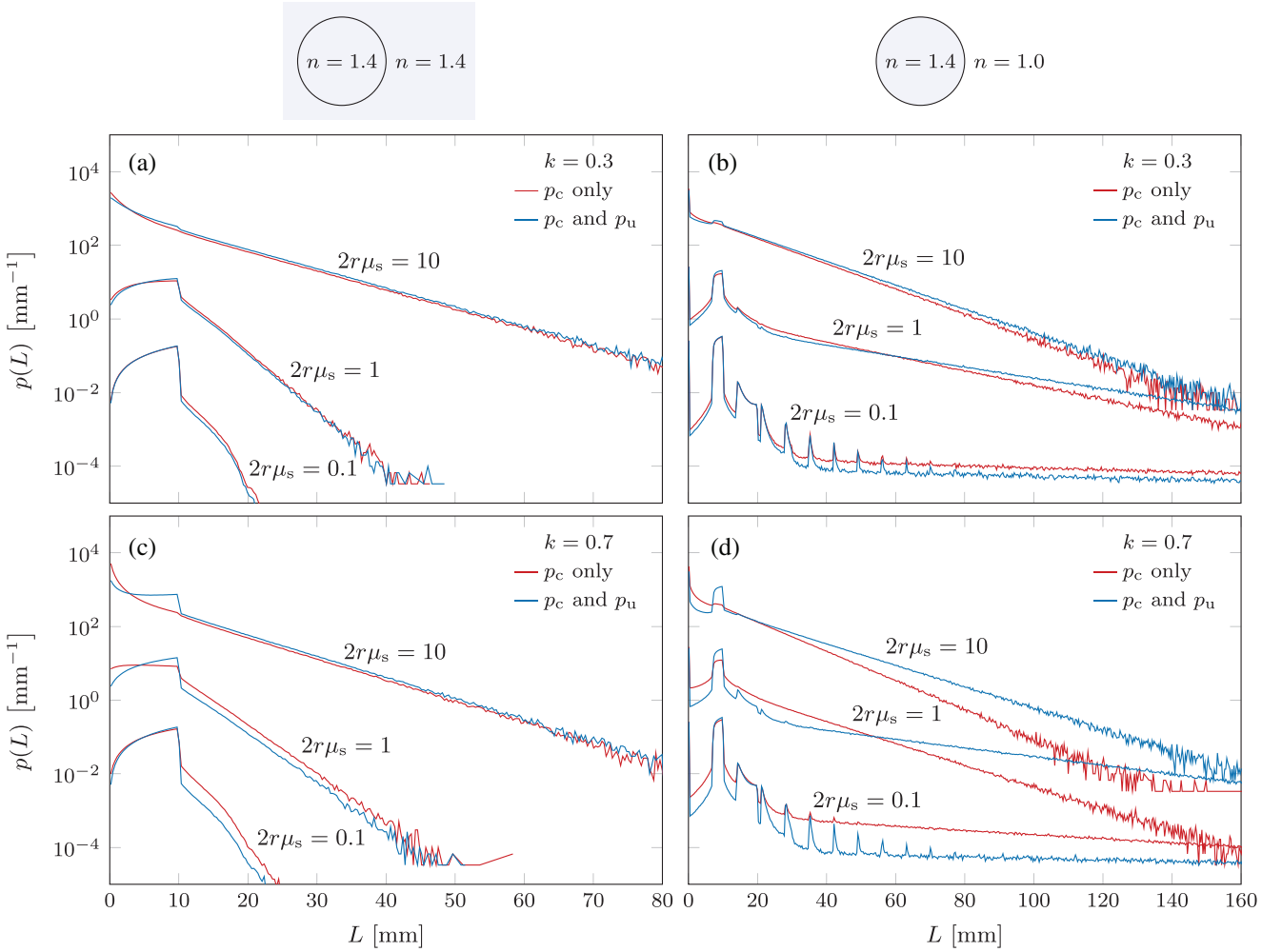

Figure 4. Comparison between total pathlength distributions obtained for a homogeneous non-absorbing sphere of radius r and refractive index $n = 1.4$ under isotropic incident radiance, in the case of (a,c) matched and (b,d) mismatched refractive index with the environment. For better visibility, curve pairs related to $2r\mu_s = 1$ and 10 are rescaled by factors of 10^2 and 10^4, respectively.

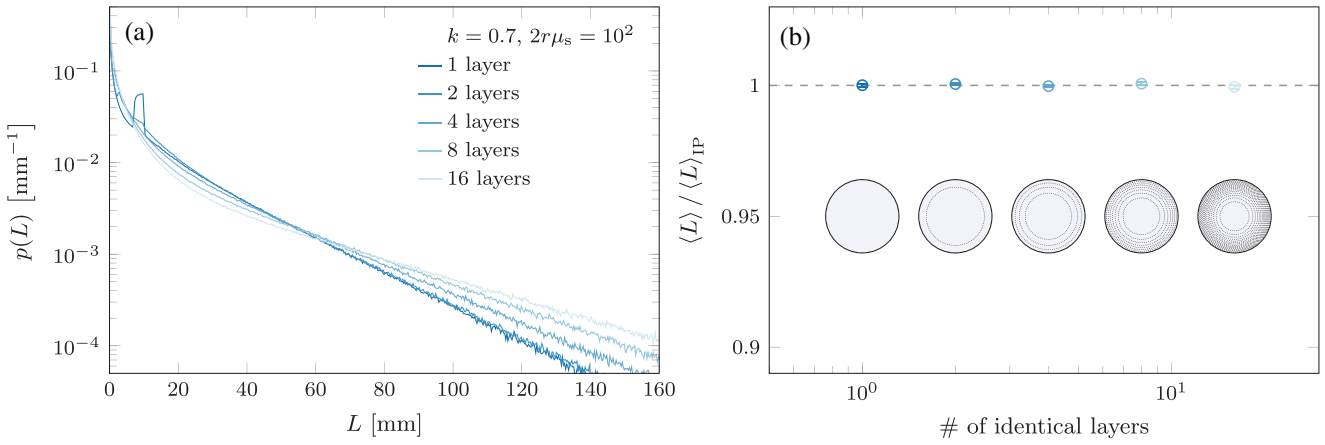

Figure 5. a) Probability density function $p(L)$ and b) normalized average pathlength $\langle L\rangle/\langle L\rangle_{IP}$ for five non-absorbing spheres with $r = 5$ mm comprising an increasing number of identical independent layers with identical properties $k = 0.7$, $\mu_s = 1$ mm^{-1}, $n = 1.4$ and $n_0 = 1$. Results are shown only in the case where both p_c and p_u are used.

environment, and *ii*) validating the results in terms of the fluence rate, which represents the main radiometric quantity of interest in light transport applications. Our results show that, even in the context of ART, the linear dependence between the average fluence rate and the average pathlength traveled by all trajectories inside the same subvolume remains valid when the appropriate step length distribution is used after a boundary interaction.

Extending the applicability of MC simulations to index-mismatched configurations represents a significant advancement, as we show that the resulting reflection and refraction events can hugely amplify the effects of such discontinuities on the overall pathlength distributions. This stands in contrast with previous reports where a modified step length distribution was used only for the initial step,[19,21] with a correspondingly vanishing impact in the limit of multiple scattering. Conversely, our results show that such discontinuity steps can introduce macroscopic discrepancies that are even more evident in the multiple scattering limit. Notably, similar discrepancies in the observable pathlength distributions are expected to arise even in other geometries (e.g., in a slab configuration) and relaxing the isotropic and Lambertian illumination condition (e.g., for a pencil beam), facilitating the comparison with experiments.

Another significant impact of discontinuities in anomalous media that we revealed is related to the possible presence of interfaces between independent realizations of the same material. The influence of such boundaries on the pathlength distribution could in principle be validated experimentally or via quenched-disorder ray-tracing simulation of Lévy-like samples, ensuring proper truncation of the non-scattering sub-domains to avoid unintentional biasing of the relevant step-length distributions.[57–59] Even more importantly, however, the existence of these generalized boundaries can have profound implications on how several MC software tools are currently implemented. A prominent example is represented by codes with mesh- or voxel-based representations of the simulation domain,[60,61] where complex geometries are divided into millions of elementary subdomains, often with identical optical properties, which however do not necessarily represent independent realizations of the same medium. In this context, from the perspective of software implementation, it will be important to distinguish between actual generalized boundaries between elementary subdomains, and other dummy boundaries introduced only for convenience purposes, where the statistical correlations of the step length distribution should not be reset.

As a final consideration, it should be stressed that the use of the discontinuity step length distribution (1) should not be viewed an ad hoc correction for the case of anomalous transport. In fact, we have shown that it can be considered by all means as a universal rule encompassing also the classical case. Even for classical transport, in fact, introducing a discontinuity step length after each boundary interaction preserves all invariant solutions. This is due to the fact that for an exponential distribution, $p_u(\ell) = p_c(\ell)$, which may explain why the general applicability of this rule was not recognized earlier.

Due to its mathematical definition, a relevant issue with Equation (1) is that it cannot be applied to step length distributions having a diverging first moment $\langle \ell \rangle = \infty$. Such distributions can be easily defined (for instance, by setting $k > 1$ in Equation (2)), and have even been studied experimentally in certain cases.[31] However, at the moment, their use in the context of MC simulations remains undefined. Further work is needed to investigate these edge cases, for instance by testing the limitations of this approach under even more stringent constraints, or by comparing them against appropriate experimental realizations to gauge their implications for the correct description and interpretation of generalized transport processes.

Acknowledgements

L.P. acknowledges the CINECA award under the ISCRA initiative, for the availability of high performance computing resources and support (ISCRA-C "ARTTESC"), and NVIDIA Corporation for the donation of the Titan X Pascal GPU. F.M. acknowledges financial support by the European Union's - NextGenerationEU, National Recovery and Resilience Plan, MNESYS, PE0000006 (DN. 1553 11.10.2022) and PRIN 2022, DIRS, grant number: 2022EB4B7E. A.S. acknowledges financial support by the National Institutes of Health: R01 EB029414. Authors acknowledge useful discussions with Prof. Francesco Piazza and with Prof. Duccio Fanelli.

Conflict of Interest

The authors declare no conflict of interest.

Data Availability Statement

The data that support the findings of this study are openly available in zenodo at 10.5281/zenodo.11278462 reference number 11278462.

Keywords

anomalous transport, generalized radiative transfer equation, heterogeneous media, monte carlo simulations, random walks trajectories

Received: February 19, 2024
Revised: June 13, 2024
Published online: July 13, 2024

[1] M. F. Modest, S. Mazumder, *Radiative heat transfer*, Academic press, Cambridge **2021**.
[2] J. J. Duderstadt, W. R. Martin, *Transport theory*, John Wiley and Sons, New York **1979**.
[3] E. A. Codling, M. J. Plank, S. Benhamou, *J. R. Soc., Interface* **2008**, *5*, 813.
[4] S. A. Prahl, *Dosimetry Laser Rad. Med. Biol.* **1989**, *10305*, 105.
[5] A. Marshak, A. Davis, *3D radiative transfer in cloudy atmospheres*, Springer Science & Business Media, Berlin, Heidelberg **2005**.
[6] U. M. Noebauer, S. A. Sim, *Living Rev. Comput. Astrophys.* **2019**, *5*, 1.
[7] J. Klafter, I. M. Sokolov, *First steps in random walks: from tools to applications*, OUP Oxford, Oxford **2011**.
[8] K. Vynck, R. Pierrat, R. Carminati, L. S. Froufe-Pérez, F. Scheffold, R. Sapienza, S. Vignolini, J. J. Sáenz, *Rev. Mod. Phys.* **2023**, *95*, 045003.
[9] A. B. Davis, A. Marshak, *J. Quant. Spectrosc. Radiat. Transfer* **2004**, *84*, 3.
[10] L. Bachelier, Ph.D. thesis, École Normale Supérieure **1900**.
[11] K. Pearson, *Nature* **1905**, *72*, 294.
[12] A. Liemert, A. Kienle, *J. Math. Phys.* **2017**, *58*, 5.
[13] V. Zaburdaev, S. Denisov, J. Klafter, *Rev. Mod. Phys.* **2015**, *87*, 483.

[14] G. Ariel, A. Rabani, S. Benisty, J. D. Partridge, R. M. Harshey, A. Be'Er, *Nat. Commun.* **2015**, *6*, 8396.
[15] D. Brockmann, L. Hufnagel, T. Geisel, *Nature* **2006**, *439*, 462.
[16] D. Brockmann, T. Geisel, *Neurocomputing* **2000**, *32*, 643.
[17] A. Lagutin, V. Uchaikin, *Nucl Instrum. Meth. Phys. Res. Sect. B: Beam Interact. Mater. Atoms* **2003**, *201*, 212.
[18] P. Barthelemy, J. Bertolotti, D. S. Wiersma, *Nature* **2008**, *453*, 495.
[19] A. Mazzolo, *J. Phys. A: Math. Theor.* **2009**, *42*, 105002.
[20] A. Mazzolo, C. de Mulatier, A. Zoia, *J. Math. Phys.* **2014**, *55*, 083308.
[21] E. d'Eon, *J. Comput. Theor. Transp.* **2018**, *47*, 84.
[22] E. d'Eon, *J. Comput. Theor. Transp.* **2019**, *48*, 201.
[23] T. Binzoni, F. Martelli, *JOSA A* **2022**, *39*, 1053.
[24] C. deMulatier, A. Mazzolo, A. Zoia, *Europhys. Lett.* **2014**, *107*, 30001.
[25] A. Zoia, C. Larmier, D. Mancusi, *Europhys. Lett.* **2019**, *127*, 20006.
[26] M. Majic, W. R. Somerville, E. C. Le Ru, *Phys. Rev. A* **2021**, *103*, L031502.
[27] F. Martelli, F. Tommasi, L. Fini, L. Cortese, A. Sassaroli, S. Cavalieri, *J. Quant. Spectrosc. Radiat. Transfer* **2021**, *276*, 107887.
[28] F. Tommasi, L. Fini, S. Focardi, F. Martelli, G. Santini, S. Cavalieri, *Sci. Rep.* **2022**, *12*, 19800.
[29] D. Fulger, E. Scalas, G. Germano, *Phys. Rev. E* **2008**, *77*, 021122.
[30] Y. Zhang, E. M. LaBolle, K. Pohlmann, *Water Resour. Res.* **2009**, *45*, 10.
[31] J. Bertolotti, K. Vynck, L. Pattelli, P. Barthelemy, S. Lepri, D. S. Wiersma, *Adv. Funct. Mater.* **2010**, *20*, 965.
[32] A. Lagutin, A. Tyumentsev, *J. Phys.: Conf. Ser.* **2013**, *409*, 012050.
[33] T. Binzoni, F. Martelli, T. J. Kozubowski, *JOSA A* **2018**, *35*, 895.
[34] E. W. Larsen, R. Vasques, *J. Quant. Spectrosc. Radiat. Transfer* **2011**, *112*, 619.
[35] S. A. Rukolaine, *Phys. A: Stat. Mech. Appl.* **2016**, *450*, 205.
[36] R. Vasques, E. W. Larsen, *Ann. Nucl. Energy* **2014**, *70*, 292.
[37] A. Sassaroli, F. Tommasi, S. Cavalieri, F. Martelli, *Biomed. Opt. Express* **2023**, *14*, 148.
[38] A. Mazzolo, *Europhys. Lett.* **2004**, *68*, 350.
[39] R. Gorenflo, J. Loutchko, Y. Luchko, *Fract. Calculus Appl. Anal.* **2002**, *5*, 491.
[40] A. Liemert, A. Kienle, *J. Math. Chem.* **2018**, *56*, 317.
[41] Y. He, L. Peng, D. Zhang, Z. Zhao, *J. Bus. Econ. Stat.* **2022**, *40*, 852.
[42] S. Bertrand, R. Joo, R. Fablet, *PloS One* **2015**, *10*, e0132231.
[43] F. Martelli, T. Binzoni, S. Del Bianco, A. Liemert, A. Kienle, *Light Propagation Through Biological Tissue and Other Diffusive Media: Theory, Solutions, and Validation*, SPIE, Bellingham, WA **2022**.
[44] J. Bardsley, A. Dubi, *SIAM J. Appl. Math.* **1981**, *40*, 71.
[45] S. Blanco, R. Fournier, *Europhys. Lett.* **2003**, *61*, 168.
[46] R. Pierrat, P. Ambichl, S. Gigan, A. Haber, R. Carminati, S. Rotter, *Proc. Natl. Acad. Sci.* **2014**, *111*, 17765.
[47] F. Martelli, F. Tommasi, A. Sassaroli, L. Fini, S. Cavalieri, *Sci. Rep.* **2021**, *11*, 19486.
[48] F. Tommasi, L. Fini, F. Martelli, S. Cavalieri, *Phys. Rev. A* **2020**, *102*, 043501.
[49] F. Martelli, M. Bassani, L. Alianelli, L. Zangheri, G. Zaccanti, *Phys. Med. Biol.* **2000**, *45*, 1359.
[50] F. Martelli, G. Zaccanti, *Opt. Express* **2007**, *15*, 486.
[51] S. Yan, Q. Fang, *Biomed. Opt. Express* **2020**, *11*, 6262.
[52] K. M. Case, P. F. Zweifel, *Linear Transport Theory*, Addison-Wesley Publishing Company, Boston **1967**.
[53] G. Popescu, A. Dogariu, *Opt. Lett.* **1999**, *24*, 442.
[54] L. Rojas, M. Bina, G. Cerchiari, M. Escobedo-Sánchez, F. Ferri, F. Scheffold, *Eur. Phys. J. Spec. Top.* **2011**, *199*, 167.
[55] R. R. Naraghi, A. Dogariu, *Phys. Rev. Lett.* **2016**, *117*, 263901.
[56] L. Pattelli, R. Savo, M. Burresi, D. S. Wiersma, *Light: Sci. Appl.* **2016**, *5*, e16090.
[57] C. Groth, A. Akhmerov, C. Beenakker, *Phys. Rev. E* **2012**, *85*, 021138.
[58] R. Burioni, E. Ubaldi, A. Vezzani, *Phys. Rev. E* **2014**, *89*, 022135.
[59] Q. Baudouin, R. Pierrat, A. Eloy, E. Nunes-Pereira, P.-A. Cuniasse, N. Mercadier, R. Kaiser, *Phys. Rev. E* **2014**, *90*, 052114.
[60] Q. Fang, D. A. Boas, *Opt. Express* **2009**, *17*, 20178.
[61] Q. Fang, *Biomed. Opt. Express* **2010**, *1*, 165.